ACS OMEGA

http://pubs.acs.org/journal/acsodf

Article

High-Temperature Pyrolysis of *N*-Tetracosane Based on ReaxFF Molecular Dynamics Simulation

Xiaowen Yu, Chunhua Zhang,* Hanwen Wang, Yangyang Li, Yujia Kang, and Ke Yang

Cite This: *ACS Omega* 2023, 8, 20823−20833

Read Online

ACCESS | Metrics & More | Article Recommendations

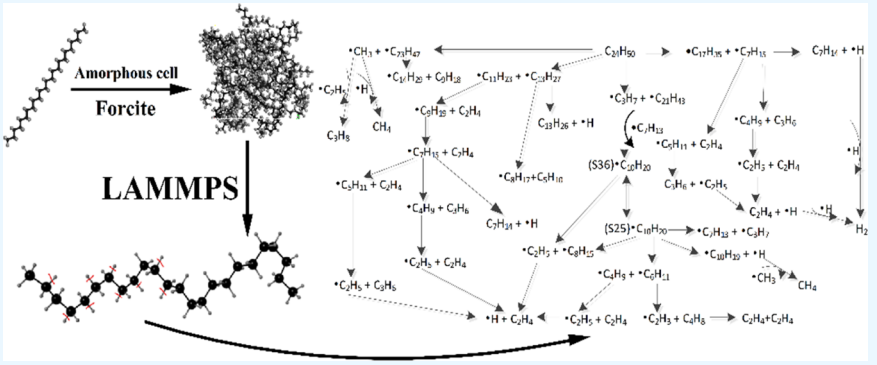

ABSTRACT: In order to further understand the high-temperature reaction process and pyrolysis mechanism of hydrocarbon fuels, the high-temperature pyrolysis behavior of *n*-tetracosane ($C_{24}H_{50}$) was investigated in this paper via the reaction force field (ReaxFF) method-based molecular dynamics approach. There are two main types of initial reaction channels for *n*-heptane pyrolysis, C−C and C−H bond fission. At low temperatures, there is little difference in the percentage of the two reaction channels. With the temperature increase, C−C bond fission dominates, and a small amount of *n*-tetracosane is decomposed by reaction with intermediates. It is found that H radicals and CH_3 radicals are widely present throughout the pyrolysis process, but the amount is little at the end of the pyrolysis. In addition, the distribution of the main products H_2, CH_4, and C_2H_4, and related reactions are investigated. The pyrolysis mechanism was constructed based on the generation of major products. The activation energy of $C_{24}H_{50}$ pyrolysis is 277.19 kJ/mol, obtained by kinetic analysis in the temperature range of 2400−3600 K.

1. INTRODUCTION

Hydrocarbon fuels play an important role in industrial production and our daily activities, the high-temperature combustion process is usually accompanied by pyrolysis. So, detailed studies of pyrolysis behavior are essential to deeply investigate the application of fuel, improve the utilization efficiency, and reduce the production of harmful species.[1−6] Pyrolysis is a very complex process, usually involving thousands of reactions, and the products of pyrolysis can also be reused to relieve the pressure of the present energy shortage.[7−9] However, it is impractical to characterize the pyrolysis process of more and more complex compounds by using only experimental and theoretical methods.

Molecular simulation is a computational chemistry method developed with the advance of computer technology and quantum chemistry to study the microscopic properties of molecules from the atomic level.[10,11] In order to make molecular dynamics simulations of large-scale chemical reaction systems practical, Van Duin et al.[12] developed a reaction force field (ReaxFF) system and it was shown that ReaxFF calculations are faster and the results are more accurate for small-molecule hydrocarbons. This also officially opened the application of ReaxFF method in the field of hydrocarbon microreactions. With the more intensive application of computational simulations, ReaxFF methods based on molecular dynamics (ReaxFF-MD) simulations have increasingly been used to study the reaction mechanisms of various fuels.[13−16] Chenoweth et al.[17] extended the ReaxFF training set in order to study the initiation reactions of hydrocarbon oxidation at high temperatures, and their study showed that the ReaxFF method can simulate the reaction process of compounds without pretreatment, which provides a new method to study the initiation reactions of hydrocarbon oxidation under extreme conditions. Page[18] and Lummen[19]

Received: March 6, 2023
Accepted: May 22, 2023
Published: June 2, 2023

used ReaxFF-MD to simulate the thermal degradation behavior of methane at low and high temperatures. This further proves the universality of the hydrocarbon reaction force field proposed by van Duin. Xin et al.[20] studied the thermal decomposition mechanism of 11 typical hydrocarbons (isobutane, isopentane, isohexane, *n*-butane, *n*-pentane, *n*-hexane, cyclobutane, cyclopentane, cyclohexane, benzene, and toluene) using the ReaxFF method based on molecular dynamics simulations and the density functional theory (DFT) method and analyzed in detail the initiating reactions of hydrocarbon pyrolysis, the effects of temperature and molecular structure on the rate of pyrolysis, and the distribution of major fragments. Ding et al.[21] explored the high-temperature pyrolysis mechanism of *n*-heptane by a series of reactive molecular dynamics simulations and calculated the apparent activation energy of *n*-heptane, which provides new insights into the application of fossil fuels. Liu et al.[22] used reaction molecular dynamics to analyze the detailed process of methylcyclohexane (MCH) pyrolysis and presented the main hydrocarbon species generated by MCH pyrolysis, initiation mechanism, intermediate reaction processes, and related kinetic behaviors. These studies prove that the ReaxFF method is outstanding in exploring the pyrolysis process and detailed reaction mechanism of low-carbon molecular structure.

However, there are many hydrocarbon fuels with long carbon chain structures. Longer carbon chain structures imply more complex reaction mechanisms, and studies have shown that the ReaxFF method is still able to describe the microscopic reaction behavior of compounds with long carbon chains in detail. Wang et al.[23] studied the initiation mechanism and kinetic behavior of *n*-dodecane combustion process using the ReaxFF-MD simulation and chemical kinetic modeling; their results showed that ReaxFF provides a reasonable oxidation reaction pathway for *n*-dodecane. Li et al.[24] studied the pyrolysis reaction of *n*-tetradecane using ReaxFF-MD simulations, which provides new ideas for understanding the effects of thermal cracking of underground crude oil. Chen et al.[25] studied the thermal cracking behavior of hexadecane at high temperatures and pressures based on ReaxFF-MD, developed the initial reaction mechanism of hexadecane, and linearly fitted the reaction activation energy of hexadecane by Arrhenius formula. Li et al.[26] studied the microscopic reaction mechanism and main products of *n*-eicosane pyrolysis and combustion based on the reactive force field molecular dynamics and proposed its detailed reaction mechanism. These studies demonstrate that ReaxFF can provide important theoretical guidance for kinetic reaction processes of hydrocarbons and simulate complex chemical processes; however, few studies have explored the microscopic reaction processes of hydrocarbons with carbon chain lengths above 20 using the ReaxFF method.

Long-chain alkanes are the main components of crude oils[27−29] as well as products produced by processing of crude oils (transportation fuels—usually below 20 carbon atoms,[30] lubricants—usually 20−40 carbon atoms,[31] heavy oils—usually 20−70 carbon atoms,[32] etc.). The study of the kinetics of alkanes with more than 20 carbon atoms is important to guide the application of lubricants or heavy oils. *N*-Tetracosane is a common structure in crude oil and lubricants.[33,34] Jin et al.[35] explored the reasons for the variation in carbon isotope values of natural gas from oil and gas reservoirs in the Tarim Basin based on the *n*-tetracosane cracking gas formation experiment. In addition, *n*-tetracosane (melting point of 51 °C) achieves renewable thermal energy storage and release as a phase change material and is a potential candidate for achieving high-temperature management.[36,37] No studies have completely described the detailed reaction mechanism about *n*-tetracosane.

Therefore, in order to provide an additional explanation of the detailed reaction mechanism of *n*-tetracosane, molecular dynamics simulations of the *n*-tetracosane at various temperatures were carried out using the ReaxFF method. Simulation results of the pyrolysis of multimolecular *n*-tetracosane are given, and the initial initiation reactions, intermediate and final product distributions, and pyrolysis kinetics of *n*-tetracosane pyrolysis are analyzed. In particular, the intermediate reaction mechanism and the detailed reaction mechanism, which cannot clearly be analyzed under the conditions of current experimental and theoretical methods, are studied in detail. The results are expected to establish the understanding of *n*-tetracosane pyrolysis from the atomic scale and provide a reliable reference for lubricant and crude oil cracking as well as practical high-temperature thermal management applications.

2. COMPUTATIONAL DETAILS

In this study, we performed simulations to investigate the pyrolysis of *n*-tetracosane using the ReaxFF method. The ReaxFF method can be used to describe chemical reaction processes in complex systems, and it describes the bond fission and formation by the bond order. We applied the CHO reaction force field proposed by van Duin,[17] which has been proven to be appropriate for application in the study of hydrocarbon systems in numerous studies.[18−26]

All simulations are repeated three times. The calculations in this study are divided into three parts. The first part is to place 20 $C_{24}H_{50}$ molecules in a cubic periodic cell through the Amorphous Cell module of Materials Studio. The size is 24.14 Å *24.14 Å *24.14 Å, the initial density of the system is 0.7991 g/cm^3, and the model establishment is shown in Figure 1.

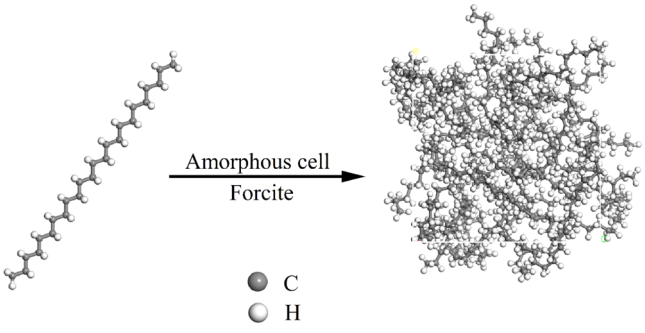

Figure 1. Model building process.

Later, the structure was optimized by the forcite module, and the optimization process used the COMPASS force field, which is proved to be suitable for the property prediction of alkane structures.[38]

The second part is the simulation calculation of the constructed model by the ReaxFF method in LAMMPS[39] for predicting the pyrolysis behavior of *n*-tetracosane. Before the simulation, the initial equilibrium model was obtained by static optimization methods, and minimizations used a conjugate gradient method with a force tolerance of 1×10^{-6} kcal/mol/Å and energy tolerance of 1×10^{-6} kcal/mol. The structure was first relaxed at 300 K for 10 ps, and at 300 K, *n*-tetracosane did

https://doi.org/10.1021/acsomega.3c01525
ACS Omega 2023, 8, 20823−20833

not cleave. The simulations were performed under the NVT (fixed number of atoms N, specified temperature T, constant volume V) ensemble, and the temperature was controlled by the Berendsen method. First, annealing simulations are performed for 1000 ps in the temperature range of 1000−3500 K to observe the pyrolysis of *n*-tetracosane in the overall temperature range. Then, simulations are performed in the temperature range of 2000−3600 K with 400 K as the interval. The final reaction mechanism is obtained from the 500 ps simulation at 3600 K. The timestep is 0.1 fs, the temperature damping coefficient is 0.05, and the critical value of the bond order for molecular recognition is set to 0.3, which is proved to be feasible in hydrocarbon-related simulations.[40]

The third part is the product distribution and mechanism analysis of LAMMPS simulation results, and the analysis was done using the ChemTrayzer (Chemical Trajectory Analyzer) code, which is based on the python code.[41]

3. RESULTS AND DISCUSSION

3.1. Multimolecular Annealing Simulation Results. In order to provide a macroscopic description of the pyrolysis of *n*-tetracosane, multimolecular annealing simulations are performed in the temperature range of 1000−3500 K from 0 ps to 1000 ps. The variation of temperature and major fragment distribution with simulation time is shown in Figure 2. The pre-equilibrated *n*-tetracosane molecule begins to

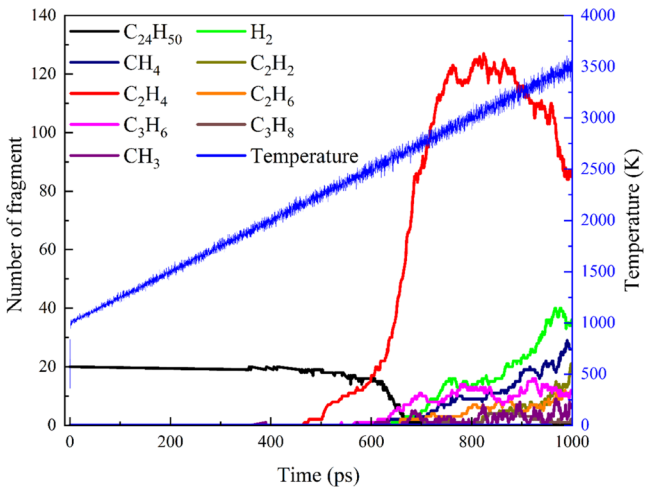

Figure 2. Result of annealing simulation.

decompose at 430 ps at a temperature of around 2021 K. The whole decomposition process of *n*-tetracosane lasts about 271 ps. According to the different decomposition rates of *n*-tetracosane, the pyrolysis of *n*-tetracosane can be divided into three stages as the temperature increases. The first stage is in the temperature range of 2091−2574 K (430−622 ps), where approximately 20% of the molecules decompose. The second stage is from 622 to 671 ps, where the temperature rises to 2654 K. The decomposition rate of *n*-tetracosane is maximum at this stage, with about 75% of the molecules decomposing. The final stage of decomposition is from 671 to 701 ps, and this stage has the slowest rate of decomposition. After 701 ps, there are no *n*-tetracosane molecules that have not yet been decomposed.

Throughout the pyrolysis process, many species are produced, in which C_2H_4 is the highest, followed by H_2 and CH_4, which is consistent with previous studies,[26] and as the simulation continues, C_2H_4 exhibits a pattern of first increasing and then decreasing. During the reduction of C_2H_4, the production of small-molecule species such as H_2 and CH_4 as well as CH_3 radicals is still on the rise. However, at the end of the simulation, 980−996 ps, the amount of H_2 shows a brief decrease, which may be due to the partial consumption of H_2 by the reaction of H_2 with the intermediate products, the main relevant reaction equation of which can be obtained in Figure 9. The amount of H_2 starts to rise slowly again at 996−1000 ps. A large number of unstable intermediates and free radicals, short-life and long-life compounds, are also observed, and these intermediates are an important source for generating small-molecule species. This suggests that small molecules, such as H_2 and CH_4, and important radicals, such as $^{\bullet}H$ and $^{\bullet}CH_3$, are partly derived from secondary decomposition.

3.2. Initial Cleavage Reaction Mechanism of *N*-Tetracosane. The initiating reactions are the basis of complex pyrolysis processes and determine the distribution of intermediate reactions and products. Particularly for long-chain alkanes, different initial conditions may form different initiation reactions. Therefore, a detailed description of the initiation reaction channel is necessary to establish the mechanism of pyrolysis of *n*-tetracosane. To investigate the different initial reactions of *n*-tetracosane at different temperatures, simulations were performed with 300 ps at 400 K intervals in the temperature range of 2000−3600 K. The variation of the number of *n*-tetracosane molecules with time at different temperatures is shown in Figure 3. With the

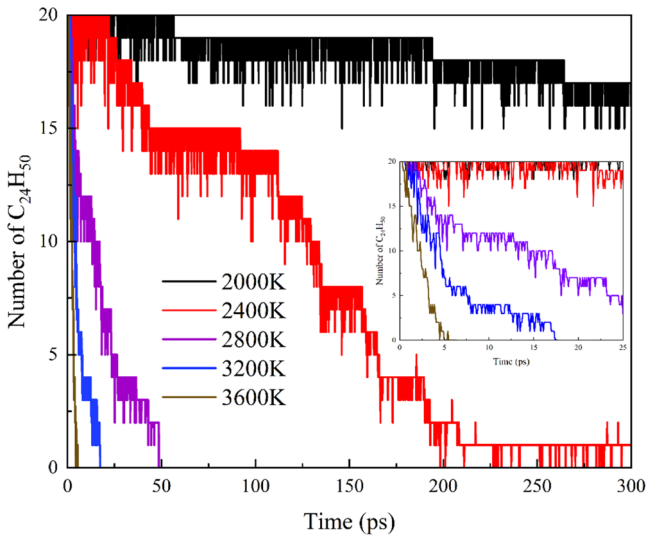

Figure 3. Change of the number of $C_{24}H_{50}$ with time at different temperatures.

increase of temperature, the consumption rate of $C_{24}H_{50}$ molecules increases significantly. As the temperature increases, the decomposition of $C_{24}H_{50}$ starts earliest, and the higher the temperature, the shorter the time for complete decomposition. As shown in Figure 4, the decomposition of $C_{24}H_{50}$ can be divided into three stages, the first stage is the stable period of $C_{24}H_{50}$ without decomposition, the second stage is the process of $C_{24}H_{50}$ decomposition, and at the third stage, $C_{24}H_{50}$ is completely decomposed and the pyrolysis process start. At 2000 K, after 300 ps of simulation, only three $C_{24}H_{50}$ molecules are completely decomposed. At 2400 K, there are

https://doi.org/10.1021/acsomega.3c01525
ACS Omega 2023, 8, 20823−20833

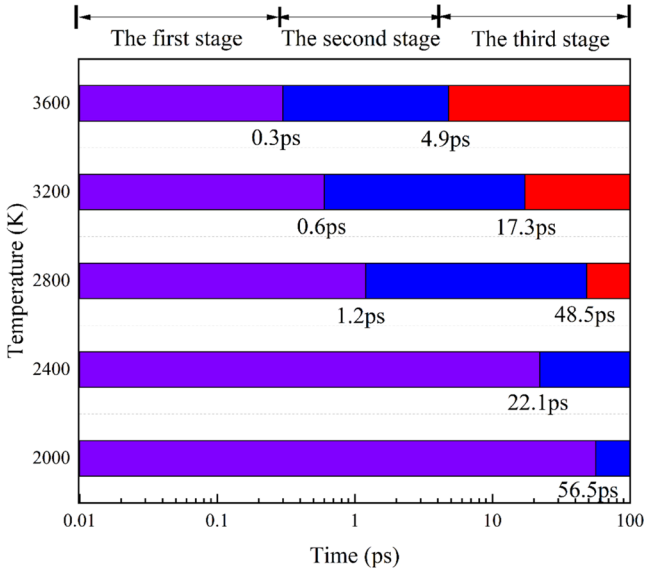

Figure 4. Different pyrolysis stages of $C_{24}H_{50}$.

19 $C_{24}H_{50}$ molecules completely decomposed. At 2800, 3200, and 3600 K, the $C_{24}H_{50}$ molecule is completely decomposed at 48.6 ps, 17.4 ps, and 5.5 ps, respectively.

The way of initial decomposition reaction of *n*-tetracosane at different temperatures is shown in Figure 5. The initial decomposition channel of *n*-tetracosane is mainly the fission of C−C bond and C−H bond. At the lower temperature of 2000 K, the ratio of the two initiation types, C−C bond fission and C−H bond fission, is not much different, and with the increase of temperature, C−C bond fission dominates. The reaction initiated by C−H fission is mainly $C_{24}H_{50} \rightarrow {}^{\bullet}C_{24}H_{49} + {}^{\bullet}H$, where all positions of C−H bond fission are shown in Figure 6. C−H bond fission occurs between the 2nd to 12th carbon atom with its connected H atom. A more specific initiation reaction occurs at higher temperatures, where the nonreacted $C_{24}H_{50}$ reacts with the formed reaction intermediates to form new reaction intermediates and small molecules. It is noteworthy that the reaction $C_{24}H_{50} + C_{24}H_{50} \rightarrow {}^{\bullet}C_{18}H_{37} + {}^{\bullet}C_{24}H_{49} + C_6H_{12} + H_2$ reaches about 4% at 3600 K. In general, under high temperatures, most of $C_{24}H_{50}$ is pyrolyzed by breaking C−C bonds to form intermediates and small molecules, a small portion of $C_{24}H_{50}$ forming ${}^{\bullet}C_{24}H_{49}$ and ${}^{\bullet}H$ by breaking C−H bonds, and the remaining small amount of still unreacted $C_{24}H_{50}$ is reacted with already formed radicals or small molecules to further produce reaction intermediates and small molecules.

3.3. Main Product Analysis. *3.3.1. Effect of Temperature on Product Species.* By analyzing the *n*-tetracosane pyrolysis products, the distribution of several major small-molecule products at different temperatures is summarized. Due to the effect of simulation temperature and simulation time, *n*-tetracosane is not completely decomposed at 2000 K. Therefore, in this section, only the distributions of small molecules at four temperatures of 2400, 2800, 3200, and 3600 K are listed, as shown in Figure 7. H_2, CH_4, C_2H_2, C_2H_4, C_2H_6, and C_3H_6 are six major small-molecule products observed in this study, which are also observed during the cleavage of *n*-alkanes of different chain lengths.[20,22,26] It is obvious from the comparison that the production of C_2H_4 is the largest and the production rate is the fastest at different temperature conditions, and its production rate increases with the increase of temperature, and the higher the temperature is, the faster the production of C_2H_4 reaches its peak. At 2400 and 2800 K, only the peak stabilization of C_2H_4 is observed. At the high temperatures of 3200 and 3600 K, C_2H_4 shows an obvious trend of first increasing and then decreasing, which is attributed to the further reaction of C_2H_4 with intermediates and the decomposition of C_2H_4 itself. At 3600 K, the amount of C_2H_4 decreases to a certain extent and then begins to stabilize. In addition, H_2 and CH_4 show higher production with increasing temperature, and a further increase in the production of H_2 and CH_4 occurs under high-temperature conditions when C_2H_4 decreases, which indicates that some of H_2 and CH_4 production is related to the consumption of C_2H_4. It is obvious that during the decomposition of *n*-tetracosane, small molecules such as C_2H_4 and C_3H_6 are produced preferentially, and the time that H_2 and C_2H_4 start to be produced does not differ much, CH_4 generally starts to be produced after H_2, and C_2H_2 and C_2H_6 molecules always start to appear at the latest moment.

3.3.2. Effect of Temperature on the Production of Major Products. At different temperatures, H_2, CH_4, and C_2H_4 are the maximum products that are produced by the pyrolysis process. The variation of H_2, CH_4, and C_2H_4 production with simulation time at different temperatures is shown in Figure 8.

Figure 8a shows the variation of H_2 production. At 2400 K, H_2 starts to be produced only at 135 ps and its production is very low. At the pyrolysis temperatures of 2800, 3200, and 3600 K, the production of H_2 starts at 15, 3, and 3 ps, respectively, and reaches the maximum values of 21, 51, and 75 at 255, 267, and 388 ps. Its production increases steadily with the increase of temperature. At 3200 and 3600 K, the amount of H_2 shows a fluctuation down state after reaching the maximum value, which is due to the reaction between H_2 and the intermediate products, where H_2 loses H atom and transforms into free-radical H, which can be confirmed by the subsequent reactions related to H_2 during the reaction.

Figure 8b shows the variation of CH_4 production. At 2400 K, the first appearance of CH_4 is at 125 ps; with the increase of temperature, the moment of first appearance of CH_4 becomes significantly earlier, and the production of CH_4 is positively proportional to both temperature and time.

Figure 8c shows the variation of C_2H_4 production. At 2400 K, the first appearance of C_2H_4 is at 9 ps. As the temperature increases, C_2H_4 appears at the beginning of the reaction around 3 ps. The rate of C_2H_4 production gradually increases with increasing temperature. At 3600 K, C_2H_4 reaches a peak at 22 ps and then declines, which can be explained by the C_2H_4-related reactions where C_2H_4 reacts with intermediates or performs secondary decomposition. C_2H_4 production stabilizes as the simulation proceeds to about 250 ps, which is the same trend as that observed previously in the annealing simulation.

3.4. Detail Analysis of *N*-Tetracosane Pyrolysis Intermediate Reaction. Although the pyrolysis reactions of various hydrocarbon structures have been studied in detail, the intermediate reactions for the cracking of long-chain alkanes are still difficult to describe directly. In this section, we analyze the intermediate reactions of *n*-tetracosane pyrolysis at the atomic level.

3.4.1. Small-Molecule Intermediate Reactions and Distribution. A total of 2065 stable and unstable intermediates are observed during the high-temperature pyrolysis of *n*-tetracosane simulated by ReaxFF-MD. This subsection

https://doi.org/10.1021/acsomega.3c01525
ACS Omega 2023, 8, 20823−20833

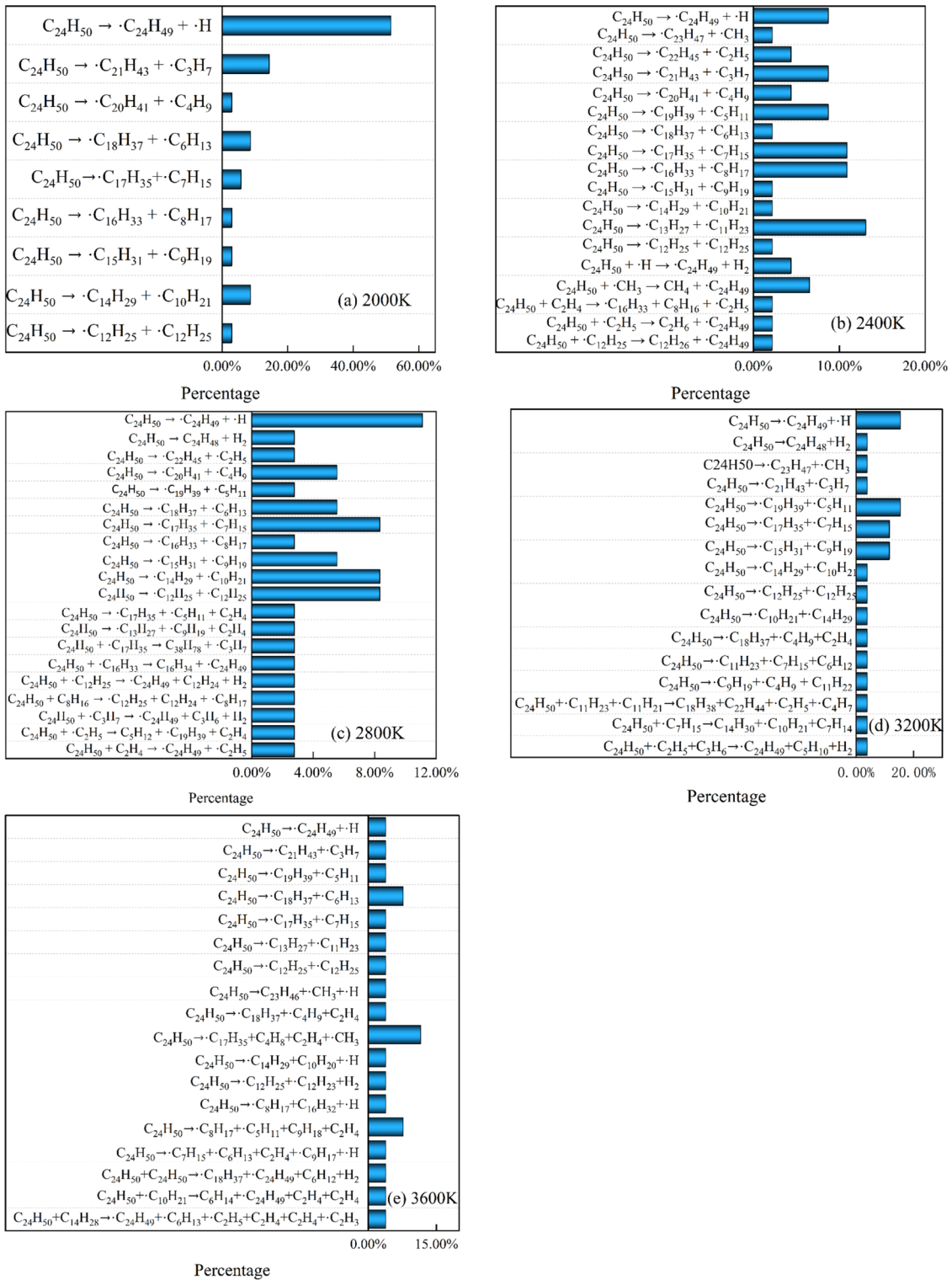

Figure 5. Way of initial decomposition reaction of *n*-tetracosane at different temperatures.

provides statistics on the relationship between the dependence of several major small-molecule production amounts on the simulation time. The production and consumption of several major products are counted at a time interval of 20 ps to explore their relevant reaction paths and reaction type distribution.

H_2 is the simplest small-molecule product in the pyrolysis of *n*-tetracosane, and it has been found in many types of reactions. It is important to understand the change rule of H_2 in the pyrolysis process to illustrate the pyrolysis process of *n*-tetracosane. The variation of H_2 production and consumption at 3600 K with time is shown in Figure 9a. The process of H_2 changes through two growth stages. The first stage is from 0 to 60 ps where H_2 production is significantly higher than consumption, and at this time, H_2 is in the growth stage. The second stage is 61−130 ps where the consumption of H_2

https://doi.org/10.1021/acsomega.3c01525
ACS Omega 2023, 8, 20823−20833

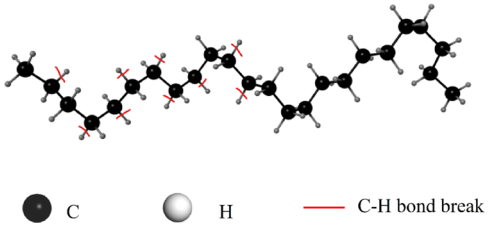

Figure 6. Position C−H bond fission.

increases significantly, gradually equal or even higher than production, and at this time, H_2 is in the stable fluctuation stage. After 130 ps, H_2 production is again higher than consumption, and the number of H_2 increases significantly. The main paths of H_2 production and consumption are shown in Figure 9b. The main path of H_2 production is $CH_4 + {}^{\bullet}H \rightarrow {}^{\bullet}CH_3 + H_2$, and its reverse reaction is the most important production path of H_2 consumption. The main pathway of the production process is H addition reaction, and H radicals are mainly derived from alkane and olefin radicals, such as ${}^{\bullet}C_2H_5$, ${}^{\bullet}C_4H_7$, etc.

CH_4 is the simplest and most abundant alkane produced during the pyrolysis of *n*-tetracosane; the variation of CH_4 is essential for an in-depth understanding of the pyrolysis mechanism of *n*-tetracosane. The time dependence of CH_4 production and consumption at 3600 K is shown in Figure 10a. A large amount of CH_4 is produced from 0 to 80 ps. During this period, the production is greater than the consumption, but due to the higher reaction temperature, the production of

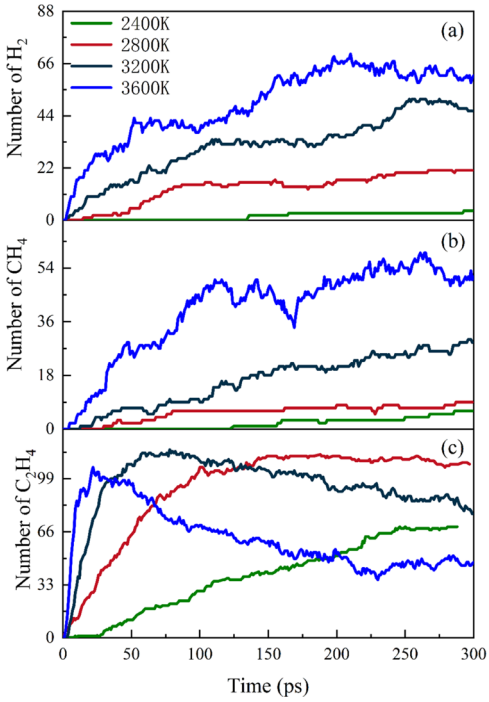

Figure 8. Effect of temperature on the production of major products.

CH_4 gradually decreases and the consumption gradually increases. From 81 to 250 ps, the consumption rate of CH_4 becomes obviously larger. After 250 ps, the production

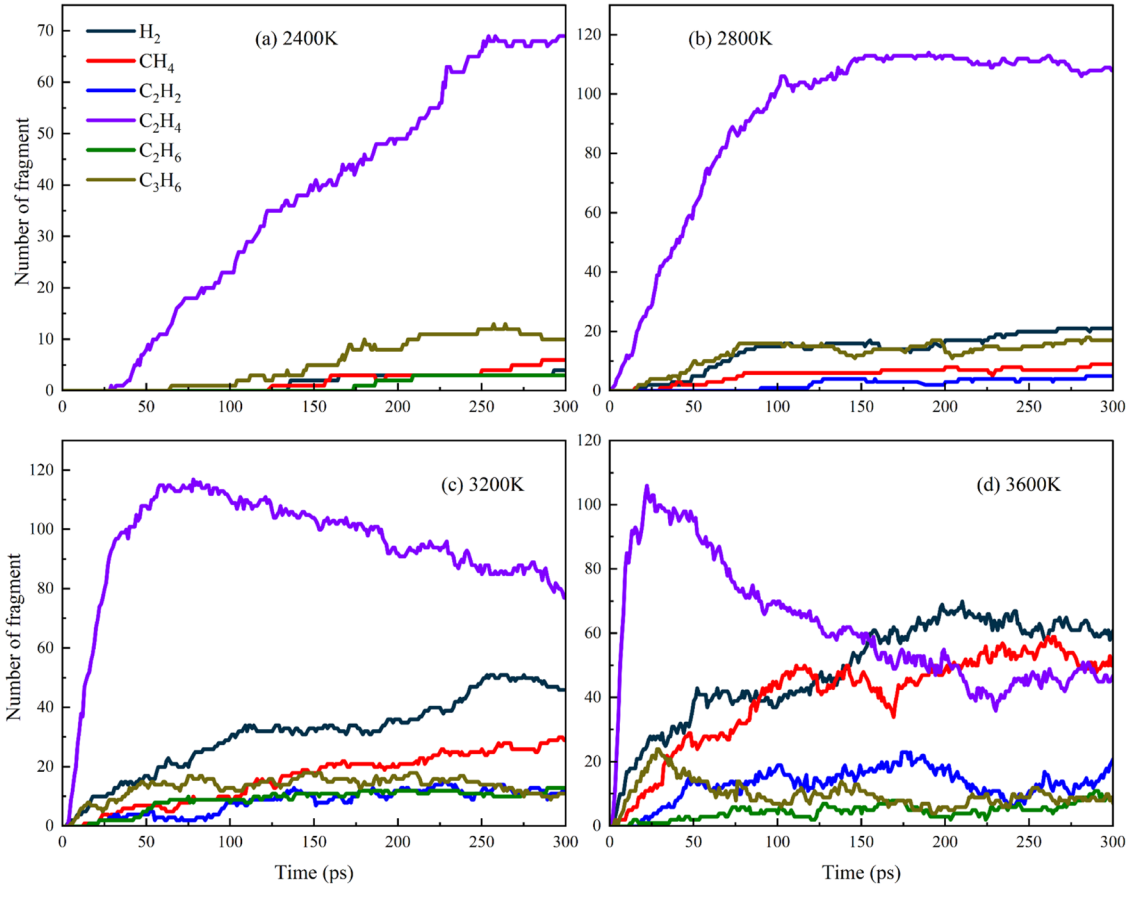

Figure 7. Distribution of main products at different temperatures.

https://doi.org/10.1021/acsomega.3c01525
ACS Omega 2023, 8, 20823−20833

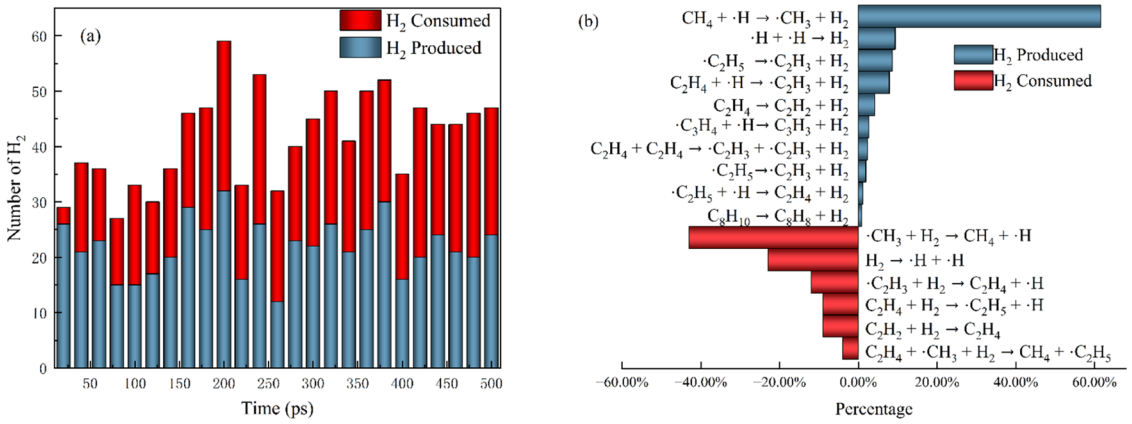

Figure 9. Intermediate reactions associated with H_2.

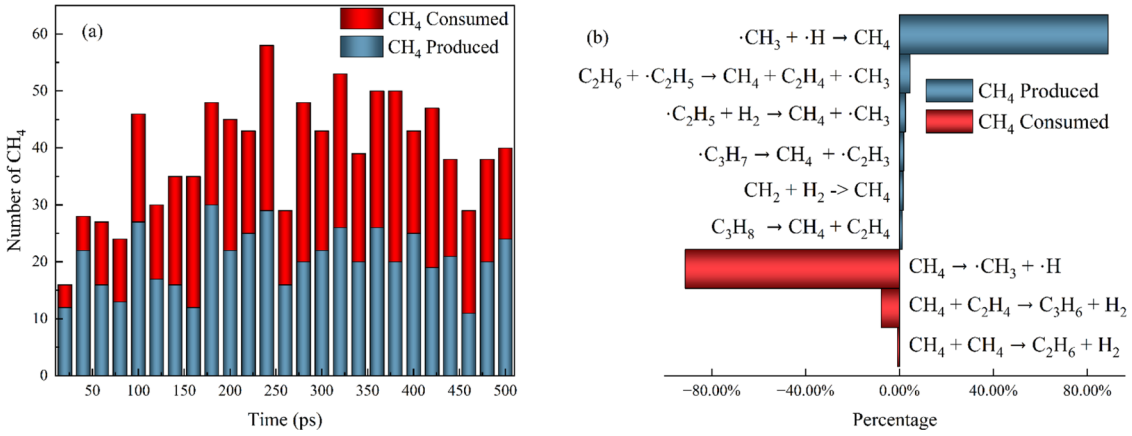

Figure 10. Intermediate reactions associated with CH_4.

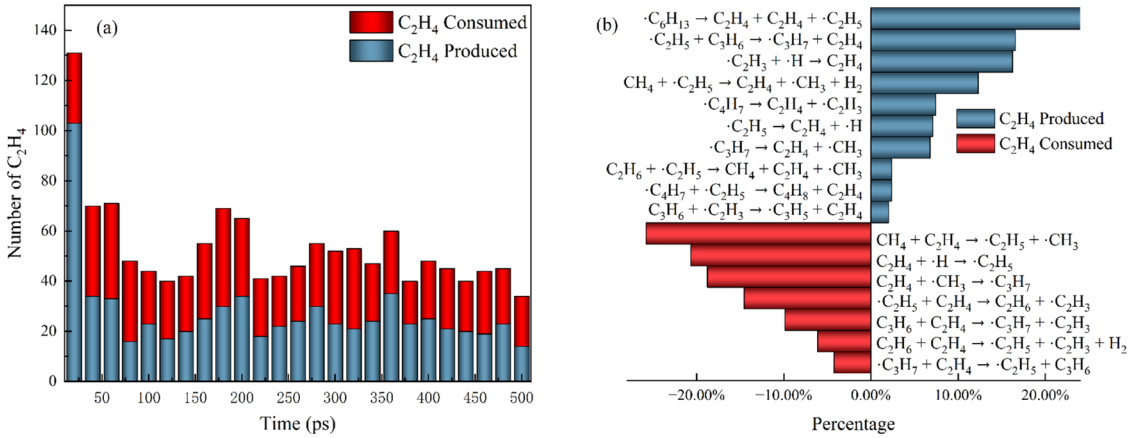

Figure 11. Intermediate reactions associated with C_2H_4.

increases significantly, the production and consumption gradually reach dynamic equilibrium, and the total number of CH_4 varies within a certain range. This change in CH_4 is mainly influenced by the methyl-related reaction pathway. The main paths of CH_4 production and consumption are shown in Figure 10b. CH_4 is formed mainly by the combination of $^{\bullet}CH_3$ with $^{\bullet}H$ and the cleavage of alkyl or alkyl radicals. The reverse reaction of $^{\bullet}CH_3 + {}^{\bullet}H \rightarrow CH_4$ is also the main pathway for CH_4 consumption. These pathways suggest that the changing conditions of CH_4 are closely related to methyl radicals. During the pyrolysis process, the general trend of CH_4 is that the production is first greater than the consumption, and after some fluctuations in the middle, it finally reaches a dynamic balance between production and consumption.

C_2H_4 is the most abundant olefin produced during the pyrolysis of *n*-tetracosane. The variation of C_2H_4 production and consumption at 3600 K with simulation time is shown in Figure 11a. The process of C_2H_4 change can be divided into three stages. The first stage is 0−20 ps, where C_2H_4 accumulates rapidly and its production reaches a peak in a short period. The second stage is 21−180 ps, when the consumption rate of C_2H_4 increases significantly and the

https://doi.org/10.1021/acsomega.3c01525
ACS Omega 2023, 8, 20823−20833

production rate decreases significantly, and this stage corresponds to the further involvement of C_2H_4 in the reaction and its production decreases significantly. The third stage is after 180 ps, where the production and consumption reactions decrease with time, and the production is slightly larger than the consumption. The main reactions of the species concerned can explain the different trends of C_2H_4 production and consumption. In the first stage, C_2H_4 is mainly generated from the dissociation of long-chain alkanes and unsaturated alkanes. Most of these reactive species come from the initial reaction channel of *n*-tetracosane pyrolysis discussed in Section 3.2, and therefore, the production of C_2H_4 may be closely related to the initial reactants. As can be seen from Figure 11b, the main source of C_2H_4 production is the fission of C−C bonds of larger hydrocarbon groups, such as $^{\bullet}C_5H_{11} \rightarrow {}^{\bullet}C_3H_7 + C_2H_4$, $^{\bullet}C_6H_{13} \rightarrow {}^{\bullet}C_2H_5 + C_2H_4 + C_2H_4$, $^{\bullet}C_8H_{17} \rightarrow C_3H_6 + C_2H_4 + C_2H_4 + {}^{\bullet}CH_3$, $^{\bullet}C_{12}H_{25} \rightarrow {}^{\bullet}C_8H_{17} + C_2H_4 + C_2H_4$, etc. H addition reactions such as $^{\bullet}C_2H_3 + {}^{\bullet}H \rightarrow C_2H_4$ are also the main reactions producing C_2H_4. The main reactions that consume C_2H_4 are $CH_4 + C_2H_4 \rightarrow {}^{\bullet}C_2H_5 + {}^{\bullet}CH_3$, where the reversible reactions, such as $C_2H_4 + {}^{\bullet}CH_3 \rightarrow {}^{\bullet}C_3H_7$, $C_2H_4 + {}^{\bullet}H \rightarrow {}^{\bullet}C_2H_5$, also have a large proportion in the process of C_2H_4 consumption, and the number of C_2H_4 reaching dynamic equilibrium in the late stage is closely related to these reversible reactions.

3.4.2. Free-Radical Distribution. Many free radicals are present during the pyrolysis of *n*-tetracosane. Small-molecule radicals play an important role in the conduct of the pyrolysis reaction. Based on the analysis of the distribution of small-molecule products in Section 3.4.1, we investigate the time dependence of the production and consumption distribution of H, CH_3, and C_2H_5 radicals, respectively.

H and CH_3 radicals have a high participation in the pyrolysis process, and the presence of radicals promotes further reactions of intermediates. Figure 12a,b shows the dependence of $^{\bullet}H$ and $^{\bullet}CH_3$ production and consumption distributions on time, respectively. At the high temperature of 3600 K, the production of $^{\bullet}H$ is slightly higher than the consumption. The reactions related to $^{\bullet}H$ do not vary much throughout the pyrolysis process, $^{\bullet}H$ is mainly produced by the decomposition reactions of alkanes or olefins, and only small amounts of H radicals are preserved as the reactions proceed. In the first 20 ps of the reaction, the production of $^{\bullet}CH_3$ is higher than the consumption, and the consumption reaction gradually increases as the simulation proceeds. $^{\bullet}CH_3$ appears more throughout the pyrolysis process, and most of $^{\bullet}CH_3$ is obtained by the $^{\bullet}H$ extraction reaction of CH_4, a small portion of $^{\bullet}CH_3$ is obtained by the direct cracking of alkanes or olefins, and $^{\bullet}CH_3$ is still present in the final product.

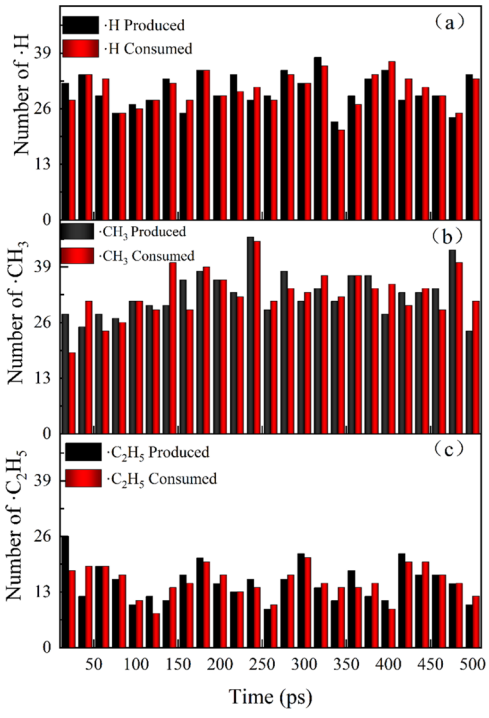

Figure 12. Small free-radical distribution of *n*-tetracosane pyrolysis.

Figure 12c shows the distribution of $^{\bullet}C_2H_5$ production and consumption dependence on time. Most $^{\bullet}C_2H_5$ production reactions occur at the beginning of the reaction, and the main channels for $^{\bullet}C_2H_5$ production are the $^{\bullet}H$ elimination decomposition reactions of C_2H_6 (such as $C_2H_6 + {}^{\bullet}H \rightarrow {}^{\bullet}C_2H_5 + H_2$) and the related reactions of intermediate reactants (such as $CH_4 + C_3H_8 + {}^{\bullet}C_3H_7 \rightarrow CH_4 + C_4H_{10} + {}^{\bullet}C_2H_5$). A small amount of $^{\bullet}C_2H_5$ is produced by C−C bond fission (such as $C_4H_{10} \rightarrow {}^{\bullet}C_2H_5 + C_2H_4 + {}^{\bullet}H$). The changes in the production and consumption reactions of $^{\bullet}C_2H_5$ proceed in parallel, so that no significant amount of $^{\bullet}C_2H_5$ exists at the end of pyrolysis.

3.5. Detailed Analysis of the Pyrolysis Mechanism. It is shown that setting higher temperature is only to speed up the simulation process and shorten the simulation time.[24−26] Section 3.3 analyzes the variation of the main products with the simulation temperature, and it can be seen that the temperature has a greater effect on the number of products generated, and the higher the temperature, the earlier the pyrolysis products appear. The effect of temperature variation on the type of pyrolysis products is not obvious, so that, according to the simulation results, the detailed reaction mechanism of *n*-tetracosane pyrolysis process at 3600 K is shown in Figure 13. It describes the detailed reaction process from the initial reactants to the most common products H_2, CH_4, and C_2H_4. The pyrolysis of $C_{24}H_{50}$ is similar to the basic long-chain alkane pyrolysis initiation reaction, which is mainly initiated by the fission of C−C bond. Many intermediates are formed during the pyrolysis process, such as $C_{10}H_{20}$ is a relatively important intermediate. These intermediates further react to form the main products. As can be seen from the reaction mechanism map, the main source of C_2H_4 is produced by the decomposition of long-chain hydrocarbon intermediates, or the H radical elimination reaction of C_2H_5 radicals. The main source of CH_4 is the H addition reaction of CH_3 radicals. The main source of H_2 is the H addition reaction of H radicals. We expect this reaction mechanism can be used to construct relevant chemical kinetic models.

3.6. Kinetic Analysis of *N*-Tetracosane Pyrolysis. To investigate the kinetic characteristics of *n*-tetracosane pyrolysis, the reaction kinetics of *n*-tetracosane was described by the consumption rate of *n*-tetracosane at temperature intervals of 400 K in the temperature range of 2400−3600 K.[42]

In our study, the concentration of *n*-tetracosane is simply replaced by the number of *n*-tetracosane molecules. The initial cleavage reaction rate (k) of *n*-tetracosane at each temperature was obtained by exponential fitting the number of decomposed *n*-tetracosane molecules. The reaction rate is calculated by eq 1

https://doi.org/10.1021/acsomega.3c01525
ACS Omega 2023, 8, 20823−20833

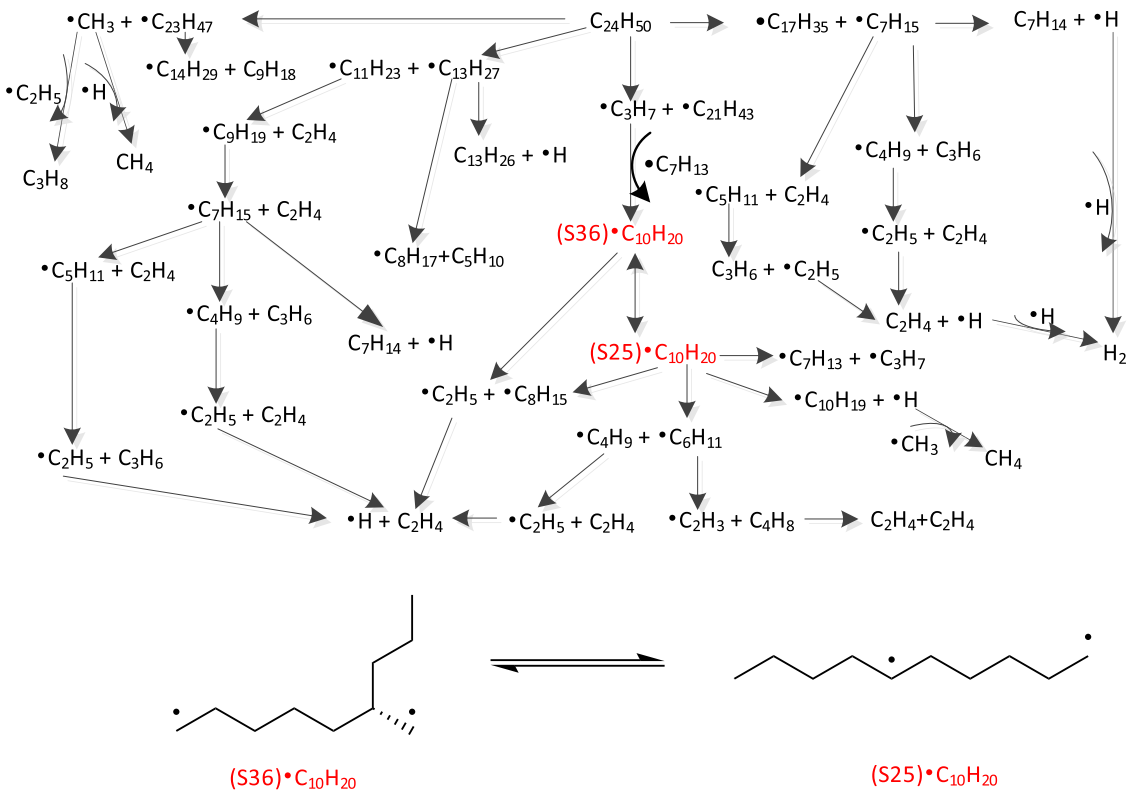

Figure 13. Detailed reaction mechanism of *n*-tetracosane pyrolysis.

$$N_t = N_0 \cdot \exp[-k(t - t_0)] \quad (1)$$

Where N_0 is the number of initial reactions of *n*-tetracosane molecules ($N_0 = 20$), t_0 is the reaction start time, and N_t is the number of molecules of *n*-tetracosane at the moment *t*.

The expression of Arrhenius formula is given by

$$k = A \exp(-E_a/RT) \quad (2)$$

Taking the logarithm gives the reaction rate k versus the activation energy E_a as a function of

$$\ln(k) = \ln(A) - \frac{E_a}{RT} \quad (3)$$

where T is the temperature, R is the gas constant, and A is the pre-exponential factor.

The Arrhenius relationship for the pyrolysis of *n*-tetracosane was obtained by fitting $\ln(k)$ to $1000/T$ as shown in Figure 14. The calculation shows that the activation energy E_a = 277.19 kJ/mol.

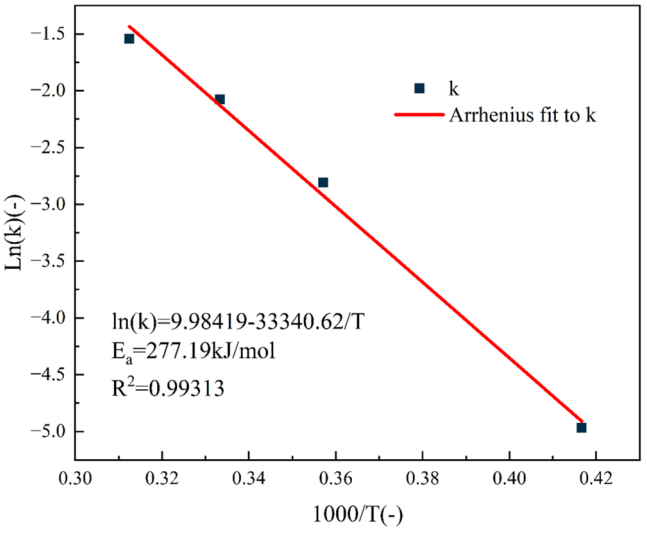

Figure 14. Kinetic analysis of *n*-tetracosane pyrolysis.

4. CONCLUSIONS

In this study, the pyrolysis of *n*-tetracosane at high temperatures is studied based on ReaxFF-MD, and the initial reaction, intermediate reaction mechanism, and product distribution associated with the pyrolysis of *n*-tetracosane are investigated, and the reaction activation energy was fitted by Arrhenius formula.

In order to describe the initial reaction process of *n*-tetracosane in detail, we discuss the initial reaction channels of *n*-tetracosane cleavage at different temperatures. There are two main types of initial decomposition of *n*-tetracosane: C−C bond and C−H bond fission. At lower temperatures, the ratios of the two initiating types, C−C bond fission and C−H bond fission, are not very different, and as the temperature increases, C−C bond fission begins to dominate. For high temperatures, a small amount of *n*-tetracosane is decomposed by reaction with intermediates due to the rapid reaction rate.

The main small-molecule products of *n*-tetracosane pyrolysis are H_2, CH_4, C_2H_2, C_2H_4, C_2H_6, and C_3H_6. C_2H_4 is the most abundant olefin, and the main source of C_2H_4 is the fission of C−C bond of the larger hydrocarbon group, and C_2H_4 reaches its peak value after the completion cleavage of $C_{24}H_{50}$, and then the content of C_2H_4 starts to decrease until it is stable. The main source of CH_4 is the H addition reaction of $^{\bullet}CH_3$, and the main source of H_2 is the H addition reaction of H radicals. The H_2 and CH_4 production continues to rise during

https://doi.org/10.1021/acsomega.3c01525
ACS Omega 2023, 8, 20823−20833

the C_2H_4 decline, suggesting that some of the H_2 and CH_4 formation is associated with the C_2H_4 reaction, which is also observed in the intermediate product-related reaction pathway. The other products such as C_3H_6 appears not far from the moment of appearance of H_2, C_2H_2 and C_2H_6 appear later, and C_2H_6 does not exist at 2000 K, which indicates that the high temperature is favorable for the formation of this product.

The apparent activation energy of *n*-tetracosane is 277.19 kJ/mol in the temperature range of 2400−3600 K fitted by Arrhenius formula. This study shows that ReaxFF is able to describe the high-temperature thermal decomposition of n-tetracosane which is expected to contribute to the thermal safety of solid hydrocarbon fuels.

AUTHOR INFORMATION

Corresponding Author

Chunhua Zhang − *Key Laboratory of Shaanxi Province for Development and Application of New Transportation Energy, Chang'an University, Xi'an 710064, China;* orcid.org/0000-0002-0349-390X; Email: zchzzz@126.com

Authors

Xiaowen Yu − *Key Laboratory of Shaanxi Province for Development and Application of New Transportation Energy, Chang'an University, Xi'an 710064, China*

Hanwen Wang − *Key Laboratory of Shaanxi Province for Development and Application of New Transportation Energy, Chang'an University, Xi'an 710064, China*

Yangyang Li − *Key Laboratory of Shaanxi Province for Development and Application of New Transportation Energy, Chang'an University, Xi'an 710064, China*

Yujia Kang − *Key Laboratory of Shaanxi Province for Development and Application of New Transportation Energy, Chang'an University, Xi'an 710064, China*

Ke Yang − *Key Laboratory of Shaanxi Province for Development and Application of New Transportation Energy, Chang'an University, Xi'an 710064, China*

Complete contact information is available at: https://pubs.acs.org/10.1021/acsomega.3c01525

Notes

The authors declare no competing financial interest.

ACKNOWLEDGMENTS

This study was supported by the Key Research and Development Program of Ningxia Hui Autonomous Region (2018BDE02057), the Innovation Capability Support Program of Shaanxi (2021TD-28), and the Special Fund for Basic Scientific Research of Central Colleges, Chang'an University (300102222502, 300102383501, 300102383502).

REFERENCES

(1) Zhang, X.; Sarathy, S. M. A lumped kinetic model for high-temperature pyrolysis and combustion of 50 surrogate fuel components and their mixtures. *Fuel* **2020**, *286*, No. 119361.

(2) Lei, Z.; Hao, S.; Yang, J.; Lei, Z.; Dan, X. Study on solid waste pyrolysis coke catalyst for catalytic cracking of coal tar. *Int. J. Hydrogen Energy* **2020**, *45*, 19280−19290.

(3) Yao, E.; Wang, Y.; Yang, Q.; Zhong, H.; Liu, T.; Zou, H.; Zhang, Y. Co-pyrolysis mechanism of natural rubber and cellulose based on thermogravimetry-gas chromatography and molecular dynamics simulation. *Energy Fuels* **2019**, *33*, 12450−12458.

(4) Hu, B.; Zhang, B.; Xie, W.; Jiang, X.; Liu, J.; Lu, Q. Recent progress in quantum chemistry modeling on the pyrolysis mechanisms of lignocellulosic biomass. *Energy Fuels* **2020**, *34*, 10384−10440.

(5) Xin, H.; Wang, H.; Kang, W.; Di, C.; Qi, X.; Zhong, X.; Wang, D.; Liu, F. The reburning thermal characteristics of residual structure of lignite pyrolysis. *Fuel* **2019**, *259*, No. 116226.

(6) Mong, G. R.; Chong, C.; Chong, W. W. F.; Ng, J. H.; Ong, H. C.; Ashokkumar, V.; Tran, M. V.; Karmakar, S.; Goh, B. H. H.; Yasin, M. F. M. Progress and challenges in sustainable pyrolysis technology: Reactors, feedstocks and products. *Fuel* **2022**, *324*, No. 124777.

(7) Chen, R.; Yu, X.; Dong, B.; Dai, X. Sludge-to-energy approaches based on pathways that couple pyrolysis with anaerobic digestion (thermal hydrolysis pre/post-treatment): Energy efficiency assessment and pyrolysis kinetics analysis. *Energy* **2019**, *190*, No. 116240.

(8) Su, G.; Ong, H. C.; Cheah, M. Y.; Chen, W. H.; Lam, S. S.; Huang, Y. Microwave-assisted pyrolysis technology for bioenergy recovery: Mechanism, performance, and prospect. *Fuel* **2022**, *326*, No. 124983.

(9) Parthasarathy, P.; Al-Ansari, T.; Mackey, H. R.; Narayanan, K. S.; McKay, G. A review on prominent animal and municipal wastes as potential feedstocks for solar pyrolysis for biochar production. *Fuel* **2022**, *316*, No. 123378.

(10) Mehana, M.; Kang, Q.; Nasrabadi, H.; Viswanathan, H. Molecular modeling of subsurface phenomena related to petroleum engineering. *Energy Fuels* **2021**, *35*, 2851−2869.

(11) Maskey, S.; Morrow, B. H.; Gustafson, M. Z.; Prak, D. J. L.; Mikulski, P. T.; Harrison, J. A. Systematic examination of the links between composition and physical properties in surrogate fuel mixtures using molecular dynamics. *Fuel* **2019**, *261*, No. 116247.

(12) Van Duin, A. C. T.; Dasgupta, S.; Lorant, F.; Goddard, W. A. ReaxFF: A reactive force field for hydrocarbons. *J. Phys. Chem. A* **2001**, *105*, 9396−9409.

(13) Liu, J.; Li, X.; Guo, L.; Zheng, M.; Han, J.; Yuan, X.; Nie, F.; Liu, X. Reaction analysis and visualization of ReaxFF molecular dynamics simulations. *J. Mol. Graphics Modell.* **2014**, *53*, 13−22.

(14) Kudinov, A. V.; Bogdanova, Y. A.; Gubin, S. A. Molecular dynamics simulation of thermal decomposition of hydrogen. *Phys. At. Nucl.* **2019**, *82*, 1486−1489.

(15) Wang, E.; Ding, J.; Qu, Z.; Han, K. Development of a reactive force field for hydrocarbons and application to iso-octane thermal decomposition. *Energy Fuels* **2018**, *32*, 1901−1907.

(16) Zheng, M.; Li, X.; Bai, J.; Guo, L. Chemical structure effects on coal pyrolyzates and reactions by using large-scale reactive molecular dynamics. *Fuel* **2022**, *327*, No. 125089.

(17) Chenoweth, K.; Van Duin, A. C. T.; Goddard, W. A. ReaxFF reactive force field for molecular dynamics simulations of hydrocarbon oxidation. *J. Phys. Chem. A* **2008**, *112*, 1040−1053.

(18) Page, A. J.; Moghtaderi, B. Molecular dynamics simulation of the low-temperature partial oxidation of CH_4. *J. Phys. Chem. A* **2009**, *113*, 1539−1547.

(19) Lümmen, N. ReaxFF-molecular dynamics simulations of non-oxidative and non-catalyzed thermal decomposition of methane at high temperatures. *Phys. Chem. Phys.* **2010**, *12*, 7883−7893.

(20) Xin, L.; Liu, C.; Liu, Y.; Huo, E.; Li, Q.; Wang, X.; Cheng, Q. Thermal decomposition mechanism of some hydrocarbons by ReaxFF-based molecular dynamics and density functional theory study. *Fuel* **2020**, *275*, No. 117885.

(21) Ding, J.; Zhang, L.; Zhang, Y.; Han, K. A reactive molecular dynamics study of n-heptane pyrolysis at high temperature. *J. Phys. Chem. A* **2013**, *117*, 3266−3278.

(22) Liu, Y.; Ding, J.; Han, K. Molecular dynamics simulation of the high-temperature pyrolysis of methylcyclohexane. *Fuel* **2018**, *217*, 185−192.

(23) Wang, Q.-D.; Wang, J.; Li, J.; Tan, N.; Li, X. Reactive molecular dynamics simulation and chemical kinetic modeling of pyrolysis and combustion of n-dodecane. *Combust. Flame* **2011**, *158*, 217−226.

(24) Li, M.; Han, Q.; Liu, X.; Xu, J.; Chen, H.; Ma, Y. New insights into the pyrolysis of n-tetradecane using ReaxFF molecular dynamics

simulations: Implications for understanding the thermal cracking of subsurface crude oil. *Energy Explor. Exploit.* **2023**, *41*, 44−61.
(25) Chen, Z.; Sun, W.; Zhao, L. High-temperature and high-pressure pyrolysis of hexadecane: Molecular dynamic simulation based on Reactive Force Field (ReaxFF). *J. Phys. Chem. A* **2017**, *121*, 2069−2078.
(26) Li, W.; Yu, S.; Zhang, L.; Chen, J.; Cao, W.; Lan, Y. ReaxFF molecular dynamics simulations of n-eicosane reaction mechanisms during pyrolysis and combustion. *Int. J. Hydrogen Energy* **2021**, *46*, 38854−38870.
(27) Li, Y. P.; Pan, J.; Ma, Y. Elucidation of multiple alkane hydroxylase systems in biodegradation of crude oil n-alkane pollution by Pseudomonas aeruginosa DN1. *J. Appl. Microbiol.* **2020**, *128*, 151−160.
(28) Thontowi, A.; Yetti, E.; Yopi, Y. Medium chain and long chain alkanes hydroxylase-producing whole cell biocatalyst from marine bacteria. *Ann. Bogor.* **2018**, *22*, 12−19.
(29) Zueva, O. S.; Zvereva, E. R.; Makarova, A. O.; Galimzyanova, A. R.; Ageeva, M. V.; Onishchenko, Y. V.; Salnikov, V. V.; Turanov, A. N.; Vakhin, A. V. Influence of high-molecular n-alkane associates on rheological behavior of the crude oil residue. *Energy Fuels* **2022**, *36*, 6755−6770.
(30) Ogawa, H.; Nishimoto, H.; Morita, A.; Shibata, G. Predicted diesel ignitability index based on the molecular structures of hydrocarbons. *Int. J. Engine Res.* **2016**, *17*, 766−775.
(31) Wang, Y.; Wang, F.; Li, J.; Liang, S.; Zhou, J. Electronic properties of typical molecules and the discharge mechanism of vegetable and mineral insulating oils. *Energies* **2018**, *11*, No. 523.
(32) Ren, Q.; Dai, Z.; Zhou, H. Mesoscale simulation on colloidal structures of heavy oil. *Acta Pet. Sin.* **2013**, *29*, 86−94.
(33) Boudouh, I.; Tamura, K.; Djemai, I.; Robustillo-Fuentes, M. D.; Hadj-Kali, M. K. Solid-liquid equilibria for biphenyl plus n-tetracosane binary mixtures and n-tetracosane plus dibenzofuran plus biphenyl ternary mixtures: Experimental data and prediction with UNIFAC models. *Int. J. Thermophys.* **2022**, *43*, No. 115.
(34) Zhang, C.; Wang, H.; Yu, X.; Peng, C.; Zhang, A.; Liang, X.; Yan, y. Correlation between the molecular structure and viscosity index of CTL base oils based on ridge regression. *ACS Omega* **2022**, *7*, 18887−18896.
(35) Jin, Y.; Wilkins, R. W. T.; Tang, Y. A kinetic model of stable carbon isotope ratios in gaseous hydrocarbons generated from thermal cracking of n-tetracosane and its application to the Tarim Basin. *J. Pet. Sci. Eng.* **2010**, *70*, 44−51.
(36) Yamada, Y.; Horibe, A. Thermal properties and related core/shell structure of n-tetracosane microencapsulated by calcium carbonate. *Appl. Therm. Eng.* **2020**, *178*, No. 115512.
(37) Rao, Z.; Wang, S.; Peng, F. Self-diffusion and heat capacity of n-alkanes based phase change materials: A molecular dynamics study. *Int. J. Heat Mass Transfer* **2013**, *64*, 581−589.
(38) Sun, H. COMPASS: an ab initio force-field optimized for condensed-phase applications overview with details on alkane and benzene compounds. *J. Phys. Chem. B* **1998**, *102*, 7338−7364.
(39) Thompson, A. P.; Aktulga, H. M.; Berger, R.; Bolintineanu, D. S.; Brown, W. M.; Crozier, P. S.; Veld, P. J. I.; Kohlmeyer, A.; Moore, S. G.; Nguyen, T. D.; Shan, R.; Stevens, M. J.; Tranchida, J.; Trott, C.; Plimpton, S. J. LAMMPS-a flexible simulation tool for particle-based materials modeling at the atomic, meso, and continuum scales. *Comput. Phys. Commun.* **2021**, *271*, No. 108171.
(40) Wang, E.; Ding, J.; Qu, Z.; Han, K. Development of a reactive force field for hydrocarbons and application to iso-octane thermal decomposition. *Energy Fuels* **2018**, *32*, 901−907.
(41) Döntgen, M.; Przybylski-Freund, M. D.; Kroger, L. C.; Kopp, W. A.; Ismail, A. E.; Leonhard, K. Automated discovery of reaction pathways, rate constants, and transition states using reactive molecular dynamics simulations. *J. Chem. Theory Comput.* **2015**, *11*, 2517−2524.
(42) Jiang, D.-e.; van Duin, A. C. T.; Van Duin, A. C. T.; Goddard, W. A. Simulating the initial stage of phenolic resin carbonization via the ReaxFF reactive force field. *J. Phys. Chem. A* **2009**, *113*, 6891−6894.

https://doi.org/10.1021/acsomega.3c01525
ACS Omega 2023, 8, 20823−20833